JOURNAL OF MATERIALS SCIENCE 26 (1991) 5229–5238

Computer modelling of the origin of defects in ceramic injection moulding

Part IV *Residual stresses*

K. N. HUNT, J. R. G. EVANS
Department of Materials Technology, Brunel University, Uxbridge, Middlesex, UK
N. J. MILLS
Department of Metallurgy and Materials, University of Birmingham, Birmingham, UK
J. WOODTHORPE
T and N Technology, Cawston House, Cawston, Rugby, UK

Thermal stress profiles were calculated for injection-moulded flat discs of a zirconia–polystyrene suspension by considering the heat flow in, and elastic properties of, the suspension in the solid state. The calculated maximum tensile stress in the centre of the moulded discs could be used to predict the incidence of cracking in moulding experiments. The computer model allows the influence of material and machine parameters on residual stress profile to be explored for the simple case of an infinite flat plate. In particular, high tensile stresses are induced by low mould temperatures and high injection pressures.

1. Introduction

Defects which appear at the injection-moulding stage in ceramic suspensions take the form of voids or cracks [1, 2]. Residual stresses are capable of producing cracks during reheating or storage [3]. Previous work has successfully predicted the incidence of voids [4] in terms of the fall in pressure at the centre of the cavity after the sprue has closed by using the equation of state of the suspension [5]. As predicted, it is a general observation that voids can be removed in static pressure moulding by increasing the hold pressure [1]. However, it is an unfortunate consequence of increasing the hold pressure that as voids are removed cracks appear [1] and for large sections a pressure "window", within which defect-free mouldings are produced, may be absent.

The present work addresses the problem of residual stresses in a quantitative manner using the same materials that have been investigated previously [4–6] in an attempt to build and test a numerical model for ceramic injection moulding so that the effects of a large number of material and machine parameters can be explored on computer. In addition to the thermal properties described previously [5], a range of mechanical properties was acquired in order to execute the analysis of stresses.

The stresses that were obtained are those associated with solidification in the cavity and not the stresses created by the flow of material into the cavity. Early calculations of cooling stresses were performed for the tempering of glass plates [7, 8]. Aggarwala and Saibel [8] for example, obtained an explicit solution for residual stresses which, for slow rates of cooling, reduced to a parabolic form with tensile stresses at the centre and compressive surface stresses. Williams [9] obtained similar explicit results for the quenching of plastics.

Mills [10, 11], in the analysis of stresses in extruded polymers, used a finite difference numerical procedure so that variations in thermal diffusivity and Young's modulus with temperature could be included in the calculation. He went on to consider briefly the creation of stresses in a flat plate moulding restricted from shrinking in the plane of the plate during solidification. More complicated finite difference analyses have since been produced for the injection moulding of thermoplastics [12, 13].

All of the models yield the basic result of a parabolic stress profile with variations produced by the pressure response with time and by the rate of cooling. The models give qualitative agreement with residual stress profiles measured by several groups [14–19]. However, little direct comparison has been made.

A complete numerical model for the stresses developed during solidification in injection moulding is extremely complex and is dependent on cavity geometry. In the present work, a number of simplifications are employed in order that effects of material and machine parameters on residual stresses can be explored by sensitivity analysis. The study extends the work of Mills [10] on the extrusion of polymers to include the variations of pressure with time within the molten core of the moulding. In the first case, one-dimensional solidification is considered in which solidified layers are unrestrained at the edges. In the real situation the pressure in the core initially restrains shrinkage but decays with time. In the second case, the edges of the moulding are constrained throughout the

0022–2461/91 $03.00 + .12

solidification stage. The experimental conditions needed to produce cracks in mouldings were compared with the predicted conditions for failure.

2. Experimental procedure

2.1. Preparation of suspension

A loading of 45 vol % zirconia (HSY3.0)* was incorporated in a polystyrene (HF555)† and dibutyl phthalate blend of weight ratio 5:1. Premixing was performed in a Henschel high-speed mixer and dispersive mixing in a Betol TS40 twin screw extruder using a procedure previously described [5].

2.2. Measurement of Young's modulus and fracture stress

Young's modulus was measured using an Instron 1195 tensile testing machine following the procedure recommended by ASTM D638 for polymers using type I bars [20]. The bars were injection moulded at a set pressure of 108 MPa on a Sandretto 6GV-50 injection-moulding machine. They were stress relieved by heating to 343 K for 5 h and furnace cooling *in vacuo*. They were then radiographed. An Instron extensometer (model no. 2630-98) with a gauge length of 50 mm was used after calibration by micrometer screw gauge. The manufacturers claim a temperature-induced error of less than 1% for the extensometer. The load cell was calibrated with dead weights. A crosshead speed of 1 mm min^{-1} was used throughout. An enclosed controlled temperature environment capable of being electrically heated or cooled with liquid nitrogen was employed to obtain the variation of Young's modulus with temperature, 1 h being allowed for the cabinet to equilibrate. After inserting the samples, 10 min were allowed for the test bars to reach temperature before attaching the extensometer. A further 15 min were allowed for equilibration of the complete set up except for samples tested at 331 K for which a shorter time was used as the bars tended to creep under the weight of the extensometer. Temperature was measured to $\pm$ 0.5 K with a mercury-in-glass thermometer. The test temperatures were 270, 294, 310 and 331 K.

A similar procedure was used for the measurement of fracture stress, the extensometer being omitted. Temperatures of 270, 293, 307, 318 and 328 K were used.

2.3. Determination of Poisson's ratio

Three discs of different thicknesses between 3 and 6 mm and 31 mm diameter were compression moulded at 493 K in an ACL 5 ton mounting press with a pressure of 12 MPa and the average thickness of each disc was measured. A Teledictor 2000 ultrasonic thickness gauge was used to measure longitudinal and shear wave velocities at different locations on each disc. The rigidity modulus, G, and bulk modulus, K, were then calculated from the relationships [21]

$$G = V_s^2 \rho \quad (1)$$

and

$$K = V_l^2 \rho - \tfrac{4}{3} G \quad (2)$$

where V_s and V_l are the shear wave velocity and longitudinal wave velocity respectively and ρ is the density of the composite. Poisson's ratio, ν, was then calculated from [21]

$$\nu = \frac{3K - 2G}{2G + 6K} \quad (3)$$

2.4. Determination of coefficient of linear expansion

The linear thermal expansion of the composite was measured using a Perkin Elmer TMS1 thermomechanical analyser using a flat probe in the range 273–338 K. The apparatus was calibrated using an aluminium standard for which the expansion coefficient was taken to be 25×10^{-6} K^{-1} at 298 K [22].

Samples were prepared from compression-moulded bars by cutting and polishing the ends flat with SiC paper. Three samples were tested after stress relieving by heating to approximately 343 K and oven cooling. A heating rate of 4 K min^{-1} was used.

2.5. Injection moulding

Mouldings were produced using two reciprocating screw injection-moulding machines, a Sandretto 6GV/50 and a Negri Bossi NB90 SM290.

Two types of disc, as shown in Fig. 1, were moulded by the Negri Bossi with the settings given in Table I. Discs with and without a circumferential lip were moulded using identical conditions. Four series of discs were produced with the variables specified in Table II.

The mould walls were tapered by 2°. The cavity pressure was recorded with a Dynisco FT444DH

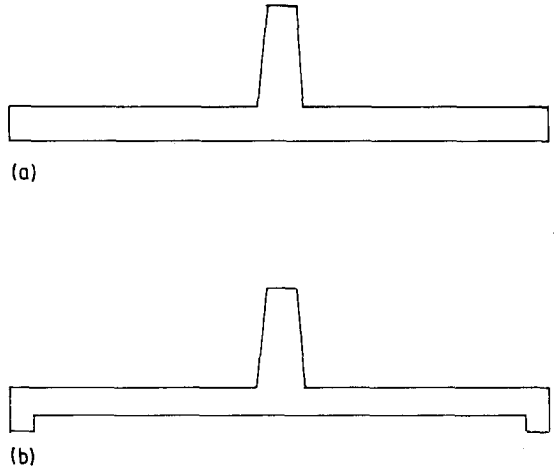

Figure 1 The injection-moulded discs in section: (a) 7 mm thick, 110 mm diameter, (b) 6 mm thick, 110 mm diameter.

*Daiichi-Kigenso, Japan
†B.P. Chemicals, UK

TABLE I Injection-moulding conditions for discs

Screw rotation speed	208 r.p.m.
Dose stop position	10.2×10^{-5} m^3
Decompression stop position	11.3×10^{-5} m^3
Feed zone temperature	463 K
Mid zone temperature	473 K
Metering zone temperature	483 K
Nozzle temperature	493 K
Nominal 1st injection speed	0.67×10^{-4} m^3 s^{-1}
Nominal 2nd injection speed	1.32×10^{-4} m^3 s^{-1} (after injecting 1.7×10^{-5} m^3)
Pressure hold time	90 s
Mould temperature	See Table II
Sprue size	See Table II

TABLE II Variable injection-moulding conditions for discs

	Series			
	1	2	3	4
Sprue diameter (mm)	6.9	6.9	10.0	10.0
Mould temperature (K)	265	313	265	313
Injection pressure = hold pressure (MPa)	10–100 variable			

force transducer. A mould temperature of 265 K was maintained by a Churchill temperature controller and a mould temperature of 313 K was maintained by a Conair Churchill 3/100 temperature controller.

3. Computation

3.1. Residual stresses in a flat plate

Residual stress profiles were predicted for injection-moulded one-dimensional polystyrene–zirconia discs by the finite difference method which is similar to the analysis of extrusion by Mills [10, 11]. A stress-free fluid subjected to a hydrostatic pressure was assumed to solidify to form an elastic solid. A composite comprising a filled glassy polymer was also assumed so that no sudden change in material properties, particularly specific volume, occurred at the solidification temperature.

The heat flow in a one-dimensional flat slab is governed by the equation

$$\frac{1}{\alpha}\frac{\partial T}{\partial t} = \frac{\partial^2 T}{\partial x^2} \tag{4}$$

This was expressed in its pure implicit finite difference form, so that

$$T(x, t + \Delta t) - T(x, t) = r[T(x + \Delta x, t + \Delta t) - 2T(x, t + \Delta t) + T(\Delta x, t + \Delta t)] \tag{5}$$

where

$$r = \alpha \Delta t / \Delta x^2 \tag{6}$$

The pure implicit method was chosen because this always produces steady decay and does not lead to the numerical oscillations associated with the Crank–Nicolson method [23].

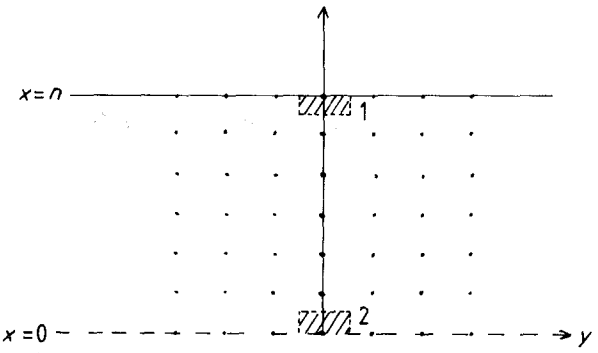

Figure 2 The grid in the section of the flat disc.

Equation 5 can be written as

$$-rT(x - \Delta x, t + \Delta t) + (1 + 2r)T(x, t + \Delta t) - rT(x + \Delta x, t + \Delta t) = T(x, t) \tag{7}$$

Owing to symmetry, only half of the thickness of the disc needs to be considered. For the present calculations this was divided into layers by 21 nodal points with node 0 on the centre line and node 20 at the mould/material interface.

Energy balance equations were written for the areas represented by the nodes at $x = 0$ (Fig. 2), the central line of symmetry and $x = n$, for the mould/material interface as follows.

For area 1 at $x = n$,

$$\rho c \frac{\Delta x \Delta y}{2}\frac{\partial}{\partial t}T(n, t) = -k\Delta y \frac{\partial T}{\partial x}\left(n - \frac{\Delta x}{2}, t + \Delta t\right)$$

heat stored — conduction into area

$$-h\Delta y[T(n, t + \Delta t) - T_m]$$

heat flow out to mould (8)

where T_m is the mould temperature, ρ is the density and c the specific heat.

For area 2 at $x = 0$

$$\rho c \frac{\Delta x \Delta y}{2}\frac{\partial}{\partial t}T(0, t) = k\Delta y \frac{\partial T}{\partial x}\left(\frac{\Delta x}{2}, t + \Delta t\right)$$

heat stored — conduction out of area (9)

Centred difference approximations were used for

$$\frac{\partial T}{\partial x}\left(n - \frac{\Delta x}{2}, t + \Delta t\right) \tag{10}$$

and

$$\frac{\partial T}{\partial x}\left(\frac{\Delta x}{2}, t + \Delta t\right) \tag{11}$$

and forward difference approximations were used for the time derivatives. Equations 8 and 9 can be rewritten, respectively, as

$$-2rT(n - 1, t + \Delta t) + (1 + 2r + 2H)T(n, t + \Delta t) = T(n, t) + 2HT_m \tag{12}$$

where

$$H = \frac{h\Delta t}{\rho c \Delta x}$$

and

$$(1 + 2r)\,T(0, t + \Delta t) - 2r\,T(1, t + \Delta t) = T(0, t) \quad (13)$$

Equations 7, 8 and 13 were written as a tridiagonal matrix equation

$$\begin{bmatrix} 1+2r & -2r & & \\ -r & 1+2r & -r & \\ & -r & 1+2r & -r \\ & & -2r & 1+2r+2H \end{bmatrix} \begin{bmatrix} T_0 \\ T_1 \\ T_2 \\ T_n \end{bmatrix}^{t+\Delta t} = \begin{bmatrix} T_0 \\ T_1 \\ T_2 \\ T_n + 2HT_m \end{bmatrix}^{t} \quad (14)$$

This was solved after each time step, Δt, using the algorithm previously described [4].

The material was assumed to be a fluid above T_g under a hydrostatic pressure and unable to sustain any stresses. As the temperature of the material passes through T_g it solidifies to an elastic solid with pressure acting on it as depicted in Fig. 3.

Prior to sprue solidification, the pressure in the moulding was assumed to be equal to the holding pressure. At the time when the sprue solidified the specific volume of material in each molten layer was calculated using the Spencer and Gilmore equation of state [5]. While a positive pressure existed in the moulding, these specific volumes were taken to be constant which assumes no mass transport occurs within the core of the moulding as solidification proceeds. After each time step and consequent temperature fall, the pressure in each layer was calculated and the average obtained. When zero pressure was reached, the pressure was assumed to remain at zero as the solid walls move freely inwards.

After each layer of material solidified, the thickness of each previously solidified layer was calculated from the relationship

$$b(i) = \Delta x + \Delta x\left[\alpha[T(i) - T_g] - \frac{1 - 2\nu}{E(i)} \times [P - PR(i)]\right] \quad (15)$$

where $b(i)$ is the thickness of layer i, Δx is the initial thickness of each layer, α is the linear thermal expansion coefficient, $T(i)$ is the temperature of layer i, $E(i)$ is Young's modulus, P is the pressure and $PR(i)$ was the pressure when layer i solidified. The change in thickness was assumed to be independent of the state of stress of the layers.

The strain in each layer was given by

$$e(i) = \frac{L - L(i)}{L(i)} = \frac{\sigma(i)(1 - \nu)}{E(i)} + \alpha[T(i) - T_g] + [P - PR(i)]\,F(E) \quad (16)$$

where $\sigma(i)$ is the stress in layer i, $L(i)$ is the initial length of each layer, that is the length L as layer i solidifies, and L is the new length at pressure P and temperature $T(i)$. $L(i)$ is given the value 1 for the outermost layer. $F(E)$ is a function of elastic modulus which approximates to $+\nu/E(i)$ for layers which have been solid for some time, corresponding to biaxial contraction as the pressure acting on them falls, and approximates to $-(1 - 2\nu)/E(i)$ for layers adjacent to the solid–liquid interface, corresponding to hydrostatic dilation.

The assumption is made that no external forces are acting for an infinite plate which has undergone shrinkage so that

$$\sum_{i=s}^{n} \sigma(i)b(i) = 0 \quad (17)$$

where layer s was the last layer to solidify. Putting $F(E) = \nu/E(i)$ this implies

$$\frac{1}{1 - \nu}\sum_{i=s}^{n} E(i)b(i)\left[\frac{L}{L(i)} - 1 - \alpha[T(i) - T_g] - [P - PR(i)]\frac{\nu}{E(i)}\right] = 0 \quad (18)$$

which gives

$$L = \sum_{i=s}^{n} E(i)b(i)\left[1 + \alpha(T(i) - T_g) + [P - PR(i)]\frac{\nu}{E(i)}\right] \Big/ \sum_{i=s}^{n} \frac{E(i)b(i)}{L(i)} \quad (19)$$

When the whole body is solid each of the initial lengths $L(i)$ is known. The temperature of each layer was then set equal to the mould temperature. The thickness of each layer was calculated using Equation 15 followed by the length using Equation 19. The pressure was taken to be zero. Finally, the resulting stress distribution was calculated using Equation 16.

3.5. Residual stresses in a flat plate with a lip

The heat flow and pressure were calculated in the same way as for the flat plate, the lip being neglected.

The shape of the flat plate with a lip is shown schematically in Fig. 1b. The lip restricts the shrinkage in the plane of the plate. The stress calculation is considerably simplified as no shrinkage occurs. The strain in each layer can be calculated from a knowledge of the pressure at the time the layer solidified, and the solidification temperature.

The strain in layer i is given by

$$e(i) = \alpha[T(i) - T_g] - [P - PR(i)]\frac{1}{3K(i)} + \sigma(i)\frac{(1 - \nu)}{E(i)} = 0 \quad (20)$$

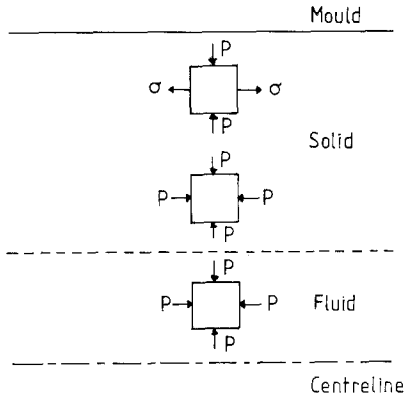

Figure 3 The stresses and pressures acting on volume elements in a one-dimensional flat disc.

where $K(i)$ is the bulk modulus of the solid in layer i given by $E(i)/3(1 - 2\nu)$, $T(i)$ is the temperature of layer i, P is the pressure and $PR(i)$ was the pressure when layer i solidified.

The stress profile was calculated at the mould temperature and zero pressure, as for the disc without a lip, so that

$$\sigma(i) = \frac{E(i)}{1 - \nu}\left[- \alpha(T_m - T_g) - PR(i)\frac{1}{3K(i)}\right] \quad (21)$$

4. Results and discussion

4.1. Mechanical properties

Radiography showed that the tensile test bars were free from macroscopic injection-moulding defects prior to testing. Elastic modulus was obtained from tangents constructed to the first straight portion of the stress–strain curve. The take up of slack was a particular problem at the high temperatures because the extensometer caused some sagging. The elastic modulus was 15 GPa at room temperature and values of elastic modulus as a function of temperature are shown in Fig. 4. For the purpose of computing, the data were fitted to straight lines within the range 270–331 K.

$$E = 15.0 \times 10^9 \quad T < 296 \quad (22)$$

$$E = 266.6 \times 10^9 - 85.00 \times 10^7 T \quad 296 \leqslant T < 312 \quad (23)$$

$$E = 24.4 \times 10^9 - 7.37 \times 10^7 T \quad 312 \leqslant T < 331 \quad (24)$$

$$E = 0 \quad T \geqslant 331 \quad (25)$$

The ultrasonic thickness gauge gave values for bulk and rigidity modulus of 12.16 and 6.74 GPa, respectively, taking the density of the suspension by rule of mixtures to be 3260 kg m^{-3}. The corresponding value of Poissons ratio is 0.27.

The fracture stress as a function of temperature is shown in Fig. 5, the room-temperature fracture stress being 18 MPa. This stress state is uniaxial and von Mises maximum shear strain energy criterion may be used to obtain a yield stress for biaxial or triaxial

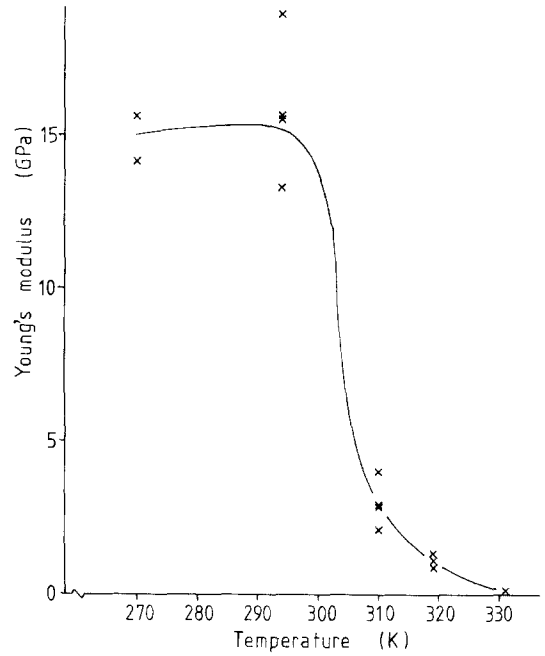

Figure 4 Elastic modulus of the suspension as a function of temperature.

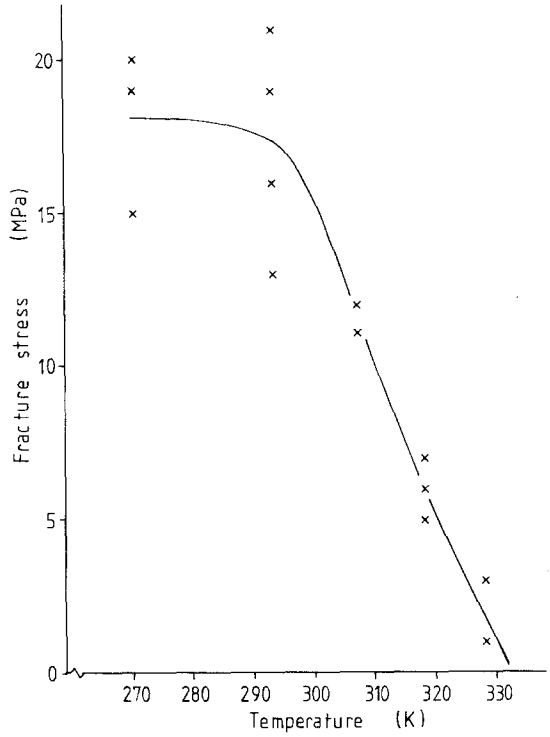

Figure 5 Fracture stress as a function of temperature.

tension [24]. This may be expressed as

$$2\sigma_0^2 = (\sigma_1 - \sigma_2)^2 + (\sigma_2 - \sigma_3)^2 + (\sigma_3 - \sigma_1)^2 \quad (26)$$

where σ_0 is the failure stress in tension and σ_1, σ_2 and σ_3 are the principal stresses. Thus in uniaxial tension $\sigma_0 = \sigma_1$ and for biaxial tension $\sigma_0 = \sigma_1 = \sigma_2$ with $\sigma_3 = 0$. Thus the fracture criterion in the centre-tensile stress distribution in the discs may be taken as the fracture stress obtained in the tensile test. It is here assumed that the similarity of manufacturing route for the discs and tensile bars provides the same distribution of critical defects for brittle fracture. The slight

effect on fracture stress of differences in effective sample volume arising from Weibull statistics is here disregarded.

4.2. Coefficient of linear expansion

Fig. 6 shows a typical dilatometric expansion curve. The non-linear behaviour exhibited by the expansion curve, particularly at higher temperatures, is mainly due to the response time of the polymer. Pure polystyrene, for example, appears to dilate and contract by two mechanisms [25]. The first is almost instantaneous with a cubical expansion coefficient of about $2.5 \times 10^{-4}\ K^{-1}$. The rate of change of dimension by the second mechanism is strongly dependent on temperature and is quite slow at room temperature, becoming more rapid as the temperature is raised. This mechanism makes an additional contribution to the cubical expansion coefficient of about $2.0 \times 10^{-4}\ K^{-1}$.

The linear expansion curve of Fig. 6 shows that the coefficient of linear expansion of the blend increases quite dramatically as T_g is approached. At 293 K the linear coefficient of expansion was $45 \times 10^{-6}\ K^{-1}$ and the softening point was approximately 330 K. This softening point may be compared with the value of T_g equal to 331 K obtained by differential scanning calorimetry.

4.3. Prediction of residual stresses and comparison with experiment: flat discs

With the cavity shown in Fig. 1a and the moulding conditions in Table I, discs were prepared with a range of pressures. A mould temperature of 265 K was used because residual stresses have been found to be sensitive to mould temperature where the latter is within 40 K of T_g [14].

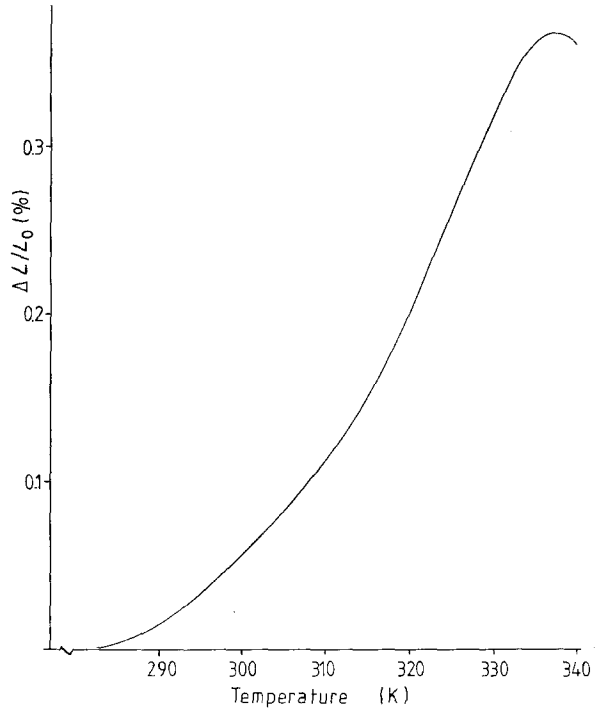

Figure 6 Dilatometric expansion for the zirconia suspension.

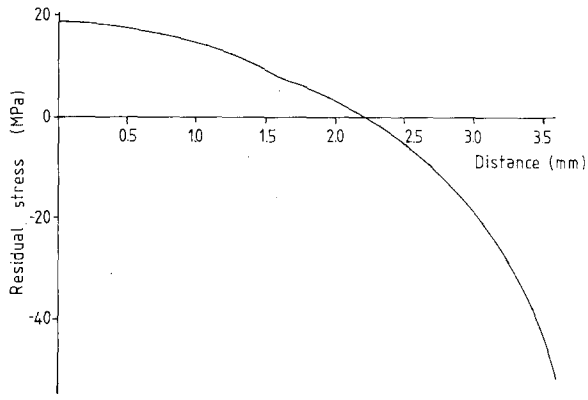

Figure 7 Residual stress distribution for a flat disc with initial cavity pressure 60 MPa, mould temperature 265 K and 10 mm diameter sprue, calculated using predicted sprue solidification time 35.9 s.

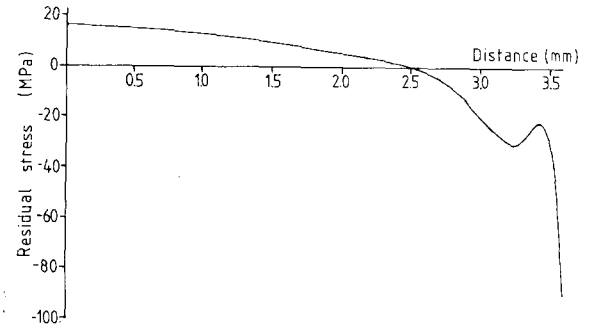

Figure 8 Residual stress distribution for a flat disc with initial cavity pressure 60 MPa, mould temperature 265 K and 6.9 mm diameter sprue, calculated using measured pressure fall-off time 5 s.

The dimensions of the mould were selected so that heat flow and stresses could be modelled in one dimension while keeping a large cross-section to reduce the influence of residual flow stresses which are expected to exist primarily at the surface [14].

As with the earlier predictions of voiding [4, 6] a difficulty exists in defining a sprue closure time. For the larger sprue, the times were calculated to be 35.9 and 59.3 s for mould temperatures 265 and 313 K, respectively. For the small sprue, the times calculated were 18.6 and 30.9 s for the mould temperatures 265 and 313 K, respectively. As before, the measured values were approximately 5 s for the small sprue and 15 s for the large sprue regardless of mould temperature. The change in the shape of the mould from the bar shape to the larger volume disc shape did not significantly affect the time at which the pressure began to fall off. This is because the pressure fall-off time is mainly dependent upon the flow properties of the blend and the radius of the sprue [6].

Stress profiles were calculated for mouldings that had been cooled to the mould temperature. Fig. 7 shows a typical stress profile predicted for material with an initial cavity pressure of 60 MPa, mould temperature 265 K and with the 10 mm diameter sprue. The sprue closure time was taken to be the calculated value of 35.9 s. The curve shows the parabolic shape typical of moulded polymers [14–18]. The stresses are higher than those typically found in moulded polymers and this is due to differences in the

thermal and mechanical properties, in particular, higher thermal diffusivity and elastic modulus.

Fig. 8 shows a second shape of stress profile predicted for the same injection pressure with a mould temperature of 265 K and with the 6.9 mm diameter sprue. The sprue cut-off time was taken to be the measured value of 5 s. In this case a compressive minimum is located just below the surface, a profile which is also typical of moulded polymers [14, 18]. In the measurement of residual stresses this surface anomaly may be confused with flow stresses but is, in fact, a consequence of changes in pressure during solidification. Figs 7 and 8 represent extremes in the sprue solidification times for the two sprue bushes used.

As with the modelling of the creation of voids [5] the uncertainty in the sprue closure time has meant that the best that can be achieved are upper and lower bounds on the injection pressures which result in a maximum tensile stress in excess of the fracture stress. For a mould temperature of 265 K the lower bound is obtained by using calculated sprue solidification time and the upper bound by using the measured time to mould cavity pressure drop. These are separated by 51 and 41 MPa for the 6.9 and 10 mm sprues, respectively.

No direct measurement of residual stress was made at this stage but it is possible to compare the predicted residual tensile stress with the measured failure stress of the material by observations of the incidence of cracking. By taking the fracture stress to be 18 MPa when the mould temperature was 265 K and 9 MPa when the mould temperature was 313 K it was possible to compare the pressure above which cracking is expected with cracks found in moulded discs. The results of this comparison are shown in Tables III and IV.

The cracks observed were present and clearly visible on ejection from the mould. The discs were also X-ray radiographed and no additional cracks were observed. Voids were found, however, in all the discs moulded at 313 K particularly near the rim where the solidification may be three dimensional. The voids may also be a source of stress relief and so although the lack of cracking in these discs agrees with the theory, the results are not conclusive. No voids were observed in any of the discs produced with mould temperature 265 K.

TABLE III Incidence of cracking as a function of initial cavity pressure

Mould temperature (K)	Sprue diameter (mm)	Pressure (MPa)	Cracks/ no cracks
265	6.9	18	N
		35	N
		51	C
		60	C
265	10	23	N
		37	C
		50	C
		62	C
313	6.9	15	N
		69	N
313	10	15	N
		36	N
		72	N

4.4. Sources of error

Several sources of error exist in the model for unrestrained discs due to the simplifications and assumptions used, notably the assumption that the moulding can be treated as an infinite plate. There is a restriction at the mould edges such that the hydrostatic dilation of recently solidified layers is not accommodated by the model in its present form.

In order to reduce the influence of flow stresses, a thickness of 7 mm was chosen while the radius of the disc was 55 mm. It is reasonable to assume with this geometry that heat flow through the edges of the disc is not significant, compared to heat flow through the flat surfaces because the diameter to thickness ratio was greater than 14:1.

Deviation from one-dimensional heat flow does occur, however, in the region near the sprue where heat transfer and hence stress state is asymmetric. Much of the cracking observed appeared random and not localized at the sprue as shown in Fig. 9. The influence of the asymmetry in this region was, therefore, not considered serious.

It was also assumed that when zero pressure was reached the walls of the moulding would move so that a negative pressure would not occur. If this were not true then voids would be expected, especially near the central plane of the disc analogous to the three-dimensional situation modelled previously [5]. Voids were observed, particularly near the edge of the mouldings produced with a mould temperature of 313 K. This is the region where the walls are likely to be restrained by solidification of the rim. No voids were observed in any mouldings produced at mould temperature 265 K.

An important difficulty which besets the analysis of residual stresses in moulded bodies is the distinction between thermal and orientation- or flow-induced stresses. The former occur during solidification while the latter originate at the mould-filling stage. A large cross-section was chosen in order to minimize the influence of flow stresses and a fast injection speed was selected for the same reason [19]. Although the injection speed was set at $1.32 \times 10^{-4}\ m^3\ s^{-1}$, the actual speed may have been lower, particularly for mouldings produced at low pressure, the injection and hold pressures being kept equal.

For the centre-gated disc-shaped mould two types of flow have been described [26]. In the radial, "r", direction the flow is mainly of the shear type while in the annular, θ, direction elongational flow occurs as the melt front increases in diameter. So in the "r" direction flow stresses are expected to be concentrated near the surface where the highest shear stresses exist, while in the θ direction a more even distribution of flow stresses would be expected as elongational flow occurs across the whole cross-section. During the long

TABLE IV

Conditions			Injection cavity pressure above which cracks are expected (MPa)	
Series	Mould temperature (K)	Sprue diameter (mm)	Predicted using calculated sprue cut-off time	Predicted using measured sprue cut-off time
1	265	6.9	46	105
2	313	6.9	$\gg 100$	$\gg 100$
3	265	10.0	15	56
4	313	10.0	$\gg 100$	$\gg 100$

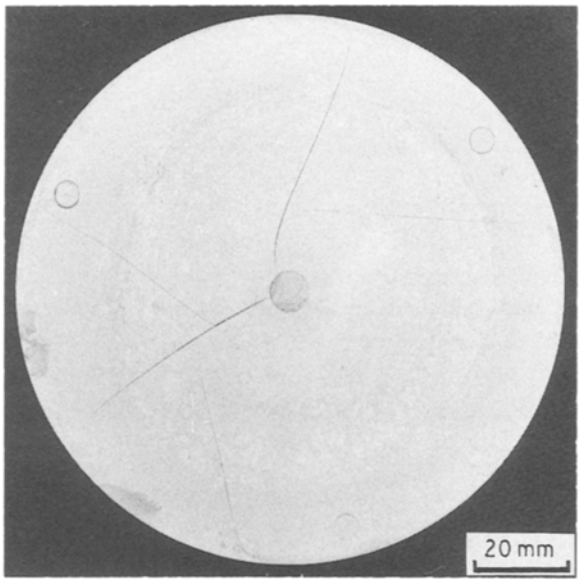

Figure 9 Photograph showing the random crack distribution in a moulded disc.

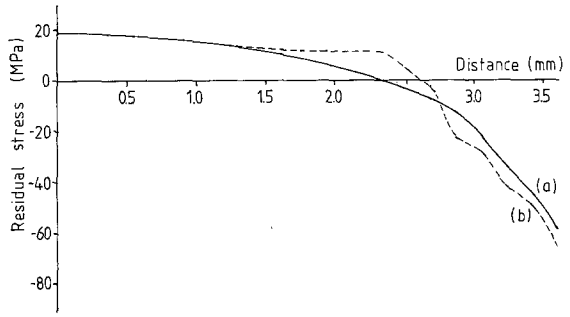

Figure 10 Residual stress distribution for a flat disc obtained with injection pressure 60 MPa, mould temperature 265 K, sprue closure time 15 s, (a) $T_g = 331$ K and $a = 45 \times 10^{-6}$ K^{-1}, and (b) $T_g = 331 + (31/100)P$ K.

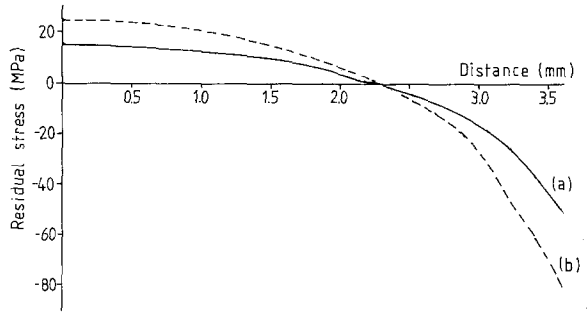

Figure 11 Residual stress distribution for a flat disc obtained with (a) $T_g = 321$ K and (b) $a = 65 \times 10^{-6}$ K^{-1}.

period of cooling, annealing of the orientation effects is expected to occur. In this case the time taken for material at the centre of the moulding to fall below T_g was greater than 40 s for a mould temperature of 265 K.

Two further sources of error that need to be considered are the effects of pressure on T_g and of stress relaxation. A 31 K rise in T_g for a pressure of 100 MPa is typical for polystyrene [27]. The effect that this has may be judged by considering as an example, material moulded with the 10 mm sprue and measured pressure fall-off time 15 s at 60 MPa and with mould temperature 265 K. The stress profile predicted for material with $T_g = 331$ K is shown in Fig. 10. By setting $T_g = 331 + (31/100)P$ the stress profile (also shown in Fig. 10) was obtained. The residual strains used to calculate the stresses in each layer were obtained by a change in temperature from T_g to the mould temperature and not from the solidification temperature. This alleviated possible problems in calculation associated with solidified material melting again as the pressure fell when a variable T_g was used. This simplification led to the uneven behaviour of the residual stress curve near the surface shown in Fig. 10. The value of the maximum tensile stress is reduced by only 0.7 MPa. This effect would be less for mouldings produced at lower pressures.

The effect of stress relaxation mechanisms below T_g may be observed by considering a reduction in the value of T_g. For example, Fig. 10 obtained with $T_g = 331$ K may be compared with Fig. 11a for material moulded under the same conditions but with $T_g = 321$ K. The maximum predicted tensile stress is reduced by 4 MPa for a 10 K reduction in T_g.

A further error exists due to the non-linearity of the thermal expansion curve discussed in Section 4.2. At 293 K the coefficient of linear expansion was 45×10^{-6} K^{-1}. Using the conditions given above, the stress profile in Fig. 10 was obtained. This may be compared with Fig. 11b obtained with an expansion coefficient of 65×10^{-6} K^{-1} which was the value measured at 308 K. The maximum predicted tensile stress is 7 MPa greater for the higher expansion coefficient.

The errors caused by stress relaxation and the non-linearity of the thermal expansion are particularly significant in this case as T_g is low, only 38 K above room temperature. The stresses developed in higher melting point blends may be more accurately determined by the present model.

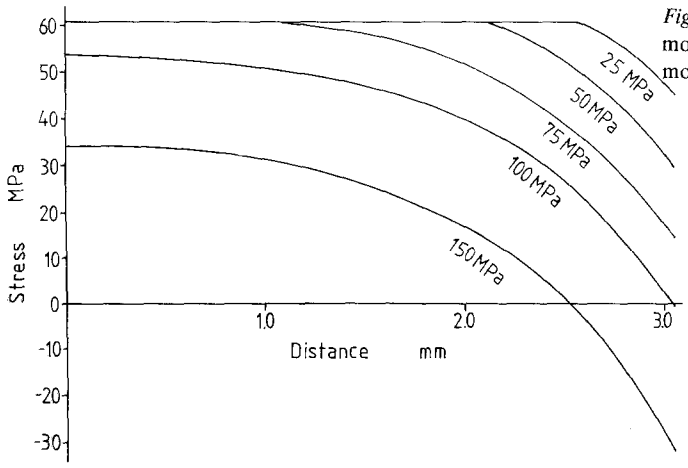

Figure 12 Residual stress distributions before removal from the mould for a flat disc with a lip with various initial cavity pressures, mould temperature 265 K and 6.9 mm diameter sprue.

4.5. Prediction of residual stresses and comparison with experiment: restrained discs

Because shrinkage is restrained in the plane of the moulding, the strain in every solidified layer at any time is zero. The moulding was assumed to remain in the mould until the temperature in every layer was equal to the mould temperature, T_m.

Typical stress profiles for material moulded at various pressures with a mould temperature of 265 K and sprue solidification time 5 s are shown in Fig. 12. The central stress is constant over several layers and is due solely to the temperature term in Equation 21 and is equal to 61 MPa. Moulding pressure decreases this stress at the surface. Because the fracture stress of the composite at this temperature was 18 MPa it is not surprising that none of the mouldings were crack free and some were removed from the mould in many small pieces.

Mouldings were also produced with a mould temperature of 313 K. With this mould temperature the thermal component of stress in Equation 21 is equal to 1.5 MPa. With an injection pressure of 14 MPa and sprue solidification times of 5 and 15 s, the stress in every layer is 1.5 MPa as the pressure reaches zero before any layers solidify. The fracture stress at this temperature was 9 MPa. Two mouldings were produced at this pressure, one using the 6.9 mm diameter sprue for which the pressure fall-off time was 5 s, and the other using the 10.0 mm diameter sprue for which the pressure fall-off time was 15 s.

The only moulding with a lip that was removed from the mould in one piece was that moulded with injection pressure 14 MPa, mould temperature 313 K and using the 10.0 mm diameter sprue. This did, however, have a fine crack around a small section of the lip and X-ray radiography revealed voids.

The moulding produced with injection pressure 14 MPa, mould temperature 313 K and using the 6.9 mm diameter sprue cracked around part of the lip. This moulding is shown in Fig. 13. It is possible that the presence of voids in these two mouldings lowered the effective fracture stress. It is also likely that some stress concentration occurred in the lip of the mouldings.

Residual stress profiles for material moulded with mould temperature 313 K, injection pressure 65 MPa and pressure fall-off times of 5 and 15 s are shown in Fig. 14. In both cases, predicted tensile stresses were less than the fracture stress yet mouldings produced with these conditions both cracked.

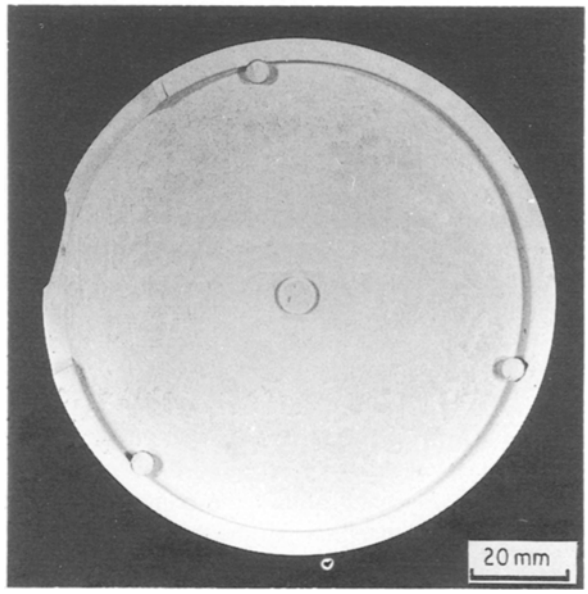

Figure 13 Photograph of moulded disc with a restraining lip.

The method used here differs significantly from that used by Mills [1] to model the solidification of polymers in a similar shape. The stresses calculated therein were the residual stresses in the plane of the moulding after removal from the mould. In order to do this, it was first assumed that no shrinkage occurs during solidification. The residual stresses after removal from the mould and cooling to room temperature were then calculated by a method similar to that of section 4.3 assuming that the sum of the stresses multiplied by the thickness of the layers equals zero. In modelling the creation of cracks, the stresses that are of importance are the maximum tensile stresses that the component is subjected to and not the stresses remaining in the part after removal from the mould.

The stresses that were calculated in this work were therefore the maximum stresses that the material encounters. They are dominated by the thermal stress as material cools from T_g to the mould temperature without shrinking. These stresses are of considerable

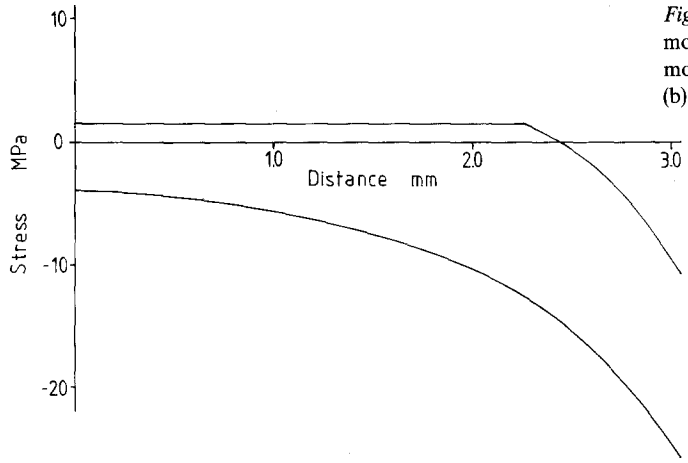

Figure 14 Residual stress distributions before removal from the mould for flat discs with lips with initial cavity pressure 65 MPa, mould temperature 313 K and (a) 10 mm diameter sprue, and (b) 6.9 mm diameter sprue.

importance in complex mould cavities where shrinkage is restrained.

5. Conclusions

Computer models have been constructed to predict the stress distribution in an infinite flat-plate moulding in terms of material and machine parameters. The models have been compared with experiment by predicting tensile failure of discs moulded from a zirconia–polystyrene suspension during cooling in the cavity. The limitations of the models in terms of, *inter alia*, the assumption of one-dimensional heat flow the simplification of strains induced by pressure decay and the neglect of flow-induced stresses are discussed. The approach allows the complex interplay of material and machine parameters to be explored rapidly on computer in advance of expensive and time-consuming laboratory investigations, but in its present form does not accurately predict stresses in mouldings.

Acknowledgements

The authors are grateful to SERC and T and N Technology for supporting this programme.

References

1. M. S. THOMAS and J. R. G. EVANS, *Brit. Ceram. Trans. J.* **87** (1988) 22.
2. M. J. EDIRISINGHE and J. R. G. EVANS, *J. Mater. Sci.* **22** (1987) 2267.
3. J. G. ZHANG, M. J. EDIRISINGHE and J. R. G. EVANS, *J. Euro. Ceram. Soc.* **5** (1989) 63.
4. K. N. HUNT, J. R. G. EVANS and J. WOODTHORPE, *J. Mater. Sci.* **26** (1991) 285.
5. *Idem, ibid.* **26** (1991) 292.
6. *Idem, ibid.* **26** (1991) 2143.
7. E. H. LEE, T. G. ROGERS and T. C. WOO, *J. Amer. Ceram. Soc.* **48** (1965) 480.
8. B. D. AGGARWALA and E. SAIBEL, *Phys. Chem. Glasses* **2** (1961) 137.
9. J. G. WILLIAMS, *Plast. Rubber Proc. Appl.* **1** (1981) 369.
10. N. J. MILLS, *J. Mater. Sci.* **17** (1982) 558.
11. *Idem, Plast. Rubber Proc. Appl.* **3** (1983) 181.
12. G. MENGES, A. DIERKES, L. SCHMIDT and E. WINKEL, *SPE Tech. Paper* **26** (1980) 300.
13. M. RIGDAHL, *Int. J. Polym. Mater.* **5** (1976) 43.
14. A. SIEGMANN, A. BUCHMAN and S. KENIG, *Polym. Engng Sci.* **22** (1982) 560.
15. A. I. ISAYEV and D. L. CROUTHAMEL, *Polym. Plast. Tech. Engng* **22** (1984) 179.
16. G. J. SANDILANDS and J. R. WHITE, *Polymer* **21** (1980) 338.
17. A. I. ISAYEV, D. L. CROUTHAMEL and K. K. WANG, *SPE ANTEC* **28** (1982) 295.
18. B. HAWORTH, C. S. HINDLE, G. J. SANDILANDS and J. R. WHITE, *Plast. Rubber Proc. Appl.* **2** (1982) 59.
19. A. I. ISAYEV and C. A. HIEBER, *Rheol. Acta* **19** (1980) 168.
20. ASTM D638 (American Society for Testing and Materials, Philadelphia, PA, 1980).
21. G. W. C. KAYE and T. H. LABY, "Tables of Physical and Chemical Constants", 13th Edn (Longman, London, 1966) p. 33.
22. "CRC Handbook of Chemistry and Physics", 67th Edn R. C. Weast (Ed.) (CRC Press, Boca Raton, Florida, 1986) D185.
23. G. E. MYERS, "Analytical Methods in Conduction Heat Transfer" (McGraw Hill, NY, 1971) pp. 281–9.
24. R. G. C. ARRIDGE, "Mechanics of Polymers" (Clarendon Press, Oxford, 1975) pp. 190–2.
25. R. S. SPENCER, in "Styrene: Its polymers, copolymers and derivatives", edited by R. H. Boundy and R. F. Boyer (Reinhold, NY, 1952) p. 602.
26. J. A. BRYDSON, "Flow properties of polymer melts", 2nd Edn (Godwin, London, 1981) pp. 118–19.
27. M. C. SHEN and A. EISENBERG, "Progress in solid state chemistry", Vol. 3, edited by H. Reiss (Pergamon Press, Oxford, 1966) p. 456.

Received 9 July
and accepted 1 August 1990